VIET NAM NATIONAL UNIVERSITY HO CHI MINH CITY
UNIVERSITY OF TECHNOLOGY

PHAM VAN ANH

DYNAMIC ANALYSIS AND MOTION CONTROL OF A FISH ROBOT DRIVEN BY PECTORAL FINS

Major: Mechanical Engineering
Major code: 62520103

SUMMARY OF PhD DESSERTATION

HO CHI MINH CITY - 2020

This dissertation is completed at the **University of Technology – VNU-HCM**

Science advisor 1: Assoc. Prof. Vo Tuong Quan, PhD
Science advisor 2: Assoc. Prof. Nguyen Tan Tien, PhD

Independent reviewer 1
Independent reviewer 2:

Reviewer 1:
Reviewer 2:
Reviewer 3:

The dissertation will be defended in front of the board of examiners at
.....
.....
on

This dissertation can be found in the libraries:

- The library of the University of Technology – VNU-HCM
- General science library - Vietnam National University – Ho Chi Minh City
- General Science Library - Ho Chi Minh City

CHAPTER 1 INTRODUCTION

1.1 General information

Some first attempts in fish-like robot research focus on anatomy structure, morphology, electromyography involving in natural fish locomotion. Similarly, the exploration in the investigations on biological fins also revealed crucial information. These are essential data for the designs such as transmissions, self-propulsive mechanisms, and turning swimming mechanisms to improve the propulsive efficiency as well as the maneuverability in the movement of the fish robot.

1.2 Motivation

Compared to biological counterparts, fish robots are still far from swimming speed, maneuverability, and efficiency. For example, the swimming speed of a robot can reach 11.6 BL/s (3.7 m/s) (Clapham and Hu 2014), while natural fish one achieves 25 BL/s (Wardle 1975). For maneuverability, the maximum turning speed of a fish robot can reach 670 deg/s (Zongshuai, Junzhi et al. 2014) is lower than 2600 deg/s of natural fish (Esox masquinongy) (Hale 2002). Additionally, the propulsive efficiency of mullet can attain 97% in continuous swimming mode. These are challenging gaps for future researches. One the other hand, fish robots propelled by the pectoral fins have high stability. However, knowledge of swimming structures employing robotic pectoral fins is very humble. Recently, an increase in pectoral fin researches has been mentioned. Some investigations have been realized on rigid pectoral fins (Kato and Furushima 1996, Kato and Inaba 1998, Sitorus, Nazaruddin et al. 2009) and uniform ones (Behbahani and Tan 2016, Behbahani and Tan 2016, Behbahani and Tan 2017). In particular, studies into robot fish, thrust by compliant structures with natural bionic shape, have not yet been regarded. Therefore, a concentration on novel pliant structures, inspired by natural pectoral fins, is necessary to implement further understanding of underwater robot designs using fin pairs. These are an excellent chance to fill the research gap by dissertation contributions.

1.3 Objective

This dissertation explores the influence of pectoral fin structures at different swimming modes on a robotic fish's locomotion behavior. Some objectives are addressed to achieve the mentioned aim as follows: Firstly, new designs based on bio-inspired pectoral fin types are constructed. Secondly, to describe fin deformation and body part movement, novel dynamically mathematical models are developed. Thirdly, experimental data are also collected and measured to complete the evaluation model, including unknown coefficients and relationships between parameters. Finally, the author compares between simulation and practical responses to examine the precision of prediction models. However, this dissertation is only limited to the fish robot's movement near the water surface and static inviscid freshwater environment.

1.4 Method and results

In this dissertation, the analysis approaches are proposed on the base of Bernoulli's theory, the Lagrange method, the Morison formula, and the rigid body dynamics. Moreover, experimental measurements, estimation of parameters, and responses comparison are performed to confirm the exactness of the proposed model. As a result, the accomplished modeling suggestion can be efficiently employed in the swimming performance analysis, optimization issues, and controller design.

1.5 Organization of dissertation

The remainder of the dissertation is organized into parts as follows. Chapter 2 presents a literature review, the proposals for filling the research gap, and the foundation theories. The procedures of modeling and motion control of the fish robot are mentioned in Chapter 3. Three types of flexible pectoral fins consisting of the uniform fins, the non-uniform fins, and the folding fins are considered in detail. Chapter 4 shows the experimental works to evaluate the proposed models. In Chapter 5, results and discussion are exhibited and evaluated. Chapter 6 summaries the novel contributions toward the fish robot area. The final is the publications.

CHAPTER 2 BACKGROUND

This chapter mentions the reports on both biology fish and robotic counterparts. It is revealed that researches on the pectoral fins of fish-like robots are not much. The considered investigations include the following edges: morphology and anatomy in the bio-inspired design of pectoral fin, kinematic and experiment, the fish robot with pectoral fin ray, modeling based numerical simulation, application of smart materials in the design of pectoral fin, experiment technique and data capturing, control issue of fish robot driven by pectoral fins, dynamic modeling, and transformation fin. From my best knowledge of the literature review, several trends and critical discussion are presented to clarify the proposed methods for solving challenges and my contributions then. This dissertation focus on flexible pectoral fins in edges of design, dynamic modeling, and motion control. Several types of flexible pectoral fins such as uniform fin, non-uniform fin, and folding fins are proposed using actuators with one DOF. Lastly, the fundamental theories concerning the Morison equation, the Rayleigh-Ritz method, the Kirchhoff's equation, and the Hammerstein Wiener estimator model are introduced.

CHAPTER 3 DYNAMIC ANALYSIS AND MOTION CONTROL

3.1 Fish robot with uniform fin flexible pectoral fins

3.1.1 The proposed model of fish robot with uniform flexible pectoral fin

To produce continuous swimming motion in lift-based mode, a design of a fish-like robot, where actuator shafts of pectoral fins are on the same straight line, was recommended. Each pectoral fin composes a rigid hinge peduncle and a flexible fin panel. This panel is constituted by uniform flexible material. The analysis schematic of the swimming movement in 2D is also demonstrated in Figure 3.1. In the body-fixed frames, the robot's motions are considered including surge (v_x), sway(v_y), and yaw (ω_z). Note that the influences of fluid on the fish body are modeled as the drag force(f_D) and lift force (f_L), and the drag moment (τ_D).

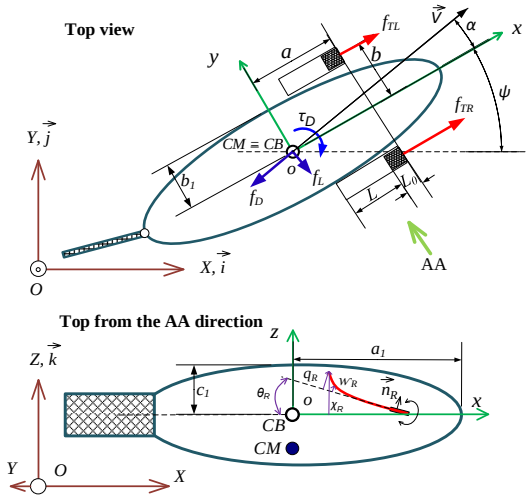

Figure 3.1 The analysis diagram of robot motion utilizing uniform pectoral fin

3.1.2 Dynamic model of uniform flexible fins

The partial differential equation expressing oscillation of a beam-like fin under the impact of the fluid force is provided as follows (Arthur W. Leissa 2011):

$$K_M \frac{\partial^4 w_K(\ell,t)}{\partial \ell^4} + \rho \frac{\partial^2 w_K(\ell,t)}{\partial t^2} + c \frac{\partial w_K(\ell,t)}{\partial t} = F_K(\ell,t), \qquad (3.1)$$

where $K_M = (1/12)Eh^3 d_0$, $\rho = m/L$, $A = d_0 L$. It notes that the subscript K refers to either R or L if the right fin or left fin is considered, respective; m is the mass of a fin. The denotations of fin sizes d_0, h, A, L are in correspondence to the thickness, the width, the area, and the length; E and c are, respectively, the Young's modulus and viscous damping coefficient; $w_K(\ell,t)$ expresses the deformation of flexible fin part K; $F(\ell,t)$ is fluid force per length unit, which acts on surface of fin. Its expression is presented by following Morison's force model (Graham 1980):

$$F_K(\ell,t) = -\frac{1}{2}\rho_H d_0 C_d v_K(\ell,t)\left|v_K(\ell,t)\right| - \frac{1}{4}\pi\rho_H d_0^2 C_a a_K(\ell,t), \qquad (3.2)$$

where ρ_H, v_K, and a_K represented the density of water, velocity and accelerate of flow, respectively.

3.1.3 Hydrodynamics of the robot body

In the horizontal plane, the swimming motion of the robot body is recommended from Kirchhoff's equation and showed in the following form (Aureli, Kopman, and Porfiri 2010):

$$\begin{cases} \left(m_b + m_x\right)\dot{v}_x = \left(m_b + m_y\right)v_y\omega_z + F_x \\ \left(m_b + m_y\right)\dot{v}_y = -\left(m_b + m_x\right)v_x\omega_z + F_y, \\ \left(J_b + J_z\right)\dot{\omega}_z = \left(m_x - m_y\right)v_x v_y + M_z \end{cases} \tag{3.3}$$

where m_b, J_b denote the mass and inertial moment of the robotic body, respectively; m_x, m_y and J_z signify coresspondingly the added masses and added inertia with respect to axes x_b, y_b and z_b.

3.1.4 Trajectory tracking control for robot motion

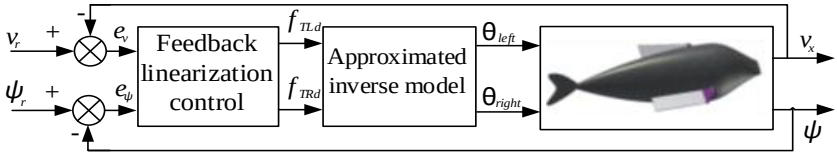

Figure 3.2 The schematic diagram of direction and velocity controller

To stabilize the direction and the surge velocity of the robot contemporaneously, a control structure is proposed as the illustration in Figure 3.2. The control law, based on feedback linearization approach, is recommended as follows:

$$\begin{bmatrix} f_{TLd} \\ f_{TRd} \end{bmatrix} = \frac{1}{2}\begin{bmatrix} 1 & -b \\ 1 & b \end{bmatrix}\begin{bmatrix} \left(m_b + m_x\right)u_v - v_y\omega_z\left(m_b + m_y\right) + f_D\cos\alpha - f_L\sin\alpha \\ \left(J_{bz} + J_r\right)u_\psi - \left(m_x - m_y\right)v_x v_y + \tau_D \end{bmatrix}, \tag{3.4}$$

where u_v and u_ψ are "equivalent inputs" and their dynamics result become linear: $\ddot{\psi} = u_\psi$, and $\dot{v}_x = u_v$. By choosing u_v, u_ψ as follows:

$$u_\psi = \ddot{\psi}_r + \lambda_1\dot{e}_\psi + e_\psi; u_v = \dot{v}_r + \lambda_2 e_v, \tag{3.5}$$

where $e_v = v_r - v_x$, $e_\psi = \psi_r - \psi$, $\dot{e}_\psi = \dot{\psi}_r - \dot{\psi}$ are the errors of surge velocity and direction angle, and velocity of direction angle error, respectively. λ_1 and λ_2 denote positive constants. The closed-loop dynamic system becomes as:

$\ddot{e}_\psi + \lambda_1 \dot{e}_\psi + e_\psi = 0$, and $\dot{e}_v + \lambda_2 e_v = 0$. The solution from this equation reveals that errors converge to zero values exponentially, i.e., $e_\psi(t) \to 0$ and $e_u(t) \to 0$ as $t \to \infty$. From equations of (3.4) and (3.5), the real control input to pectoral fin is computed. Because of the complexity of solving the fin inverse dynamic model, the Hammerstein-Wiener estimator with a simple structure and the accuracy of the outcome is recommended for replacement. This approximate model is a nonlinear estimator with parameters determined by the trial-error method.

3.2 Fish robot propelled non-uniform pectoral fins

3.2.1 Geometric design of non-uniform pectoral fin

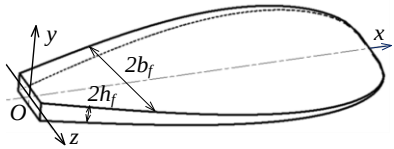

Figure 3.3 The compliant non-uniform fin profile

In natural fish, the pectoral fin shapes, which evolutes from locomotion modes, are remarkably various. They support the robot's maneuverability in the skills of braking, accelerating as well as instantaneously turning. Inspired by the natural counterpart of the snakehead fish's pectoral fin with symmetrical geometry and non-uniform, the profile of the artificial pectoral fin is recommended as Figure 3.3.

3.2.2 Dynamic model of the robotic fish with non-uniform pectoral fins

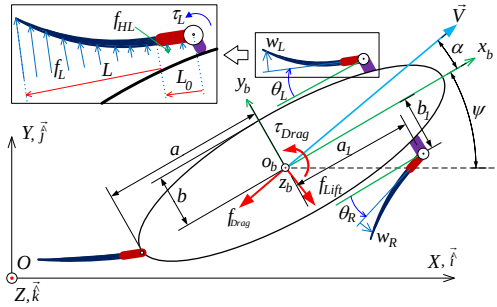

Figure 3.4 The descriptive diagram of the fish robot with non-uniform fins

In this subsection, a hydrodynamic model for both the motions of fins and the robot body is abridged. The analytical diagram of the fish robot is exhibited in Figure 3.4. w_K is the bending deflection of the flexible pectoral fin part. It is assumed that fin's deformation magnitude can be approximated by a limited series $w_K(x,t)=\sum_{k=1}^{n}\varphi_k(x)\delta_{kK}(t)$, where $\varphi_k(x)$ and $\delta_{kK}(t)$ denote the k^{th} mode shape function and the unknown functions of time, respectively. The external fluid forces over per length unit of the hinge peduncle and the flexible pectoral fin part K are respectively determined by employing Morison's formula as follows:

$$f_{HK}=-\rho_H C_a\frac{\pi}{4}d_0^2 a_{HK}-\frac{1}{2}C_d\rho_H v_{HK}d_0|v_{HK}|, \tag{3.6}$$

$$f_K=-\rho_H C_a\frac{\pi}{4}d^2 a_K-\frac{1}{2}C_d\rho_H v_K d|v_K|, \tag{3.7}$$

where d_0, d signify the widths of hinge and compliant fin part, resepctively; v_{HK}, a_{HK}, v_K and a_K are the speed and accelerate of a point corresponding to the hinge K and the flexible fin K.

By employing the Lagrange method, the differential equation of the flexible pectoral fin movement K is written as follows:

$$[M_K]\{\ddot{q}_K(t)\}+[N_K]\{q_K(t),\dot{q}_K(t)\}=\{Q_K\}, \tag{3.8}$$

where M_K and N_K are the matrixes, $q_K(t)=[\theta_K \quad ... \quad \delta_{kK} \quad ...]^T$ is the extensive coordinates, $Q_K=[Q_{0K} \quad ... \quad Q_{kK} \quad ...]^T$ is the extensively external force, $k=1,2,...,n$.

Finally, in the combination of equations (3.3) and (3.8), the equations of the robot body motion and fins displacements are exhibited in a followingly general form:

$$M(q)\ddot{q}(t)+N(q,\dot{q})=T, \tag{3.9}$$

where M refers to a term of the mass and inertia matrices, N describes force terms of Coriolis, Centripetal, and Gravity, T denotes the moment vector including the motor torques τ_K.

3.2.3 Motion control of the non-uniform pectoral fins

The amplitude modulation method is chosen because of simplicity and smoothness. On the other hand, the neutral direction of the fin angle is easy to be drifted by fluid wakes when the robot moves. To overcome this issue, the modified form of amplitude modulation approach is recommended in expression as follows:

$$\tau_K = T_m\left(1+\Delta T_K sign\left(\sin\left(2\pi ft+\gamma_K\right)\right)\right)\sin\left(2\pi ft+\gamma_K\right), \qquad (3.10)$$

here $\Delta T_K = k_\tau f_K\left(\theta_K - \theta_{dK}\right)$; k_τ is a proportional constant decided by experimental test.

3.3 Fish robot with folding pectoral fins

3.3.1 Mechanical design of folding fins

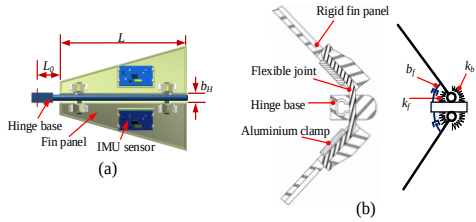

Figure 3.5 Design illustration of a flexible folding fin: the prototype of the pectoral fin (a), the equivalent model of fin elements (b)

The design of the pectoral fin on the robot is proposed in Figure 3.5. These panels are connected to the hinge base by flexible joints. In the drag-based mode, R. W. Blake (Blake 1981) claimed that propulsive production on fish is likely the triangle fins than rectangular, square, or truncated triangle ones. For this reason, a simple trapezoid for each fin panel was employed. It should be noted that the equivalent stiffnesses of the joint in "front-space" and "back-space" are denoted k_f and k_b, respectively, here $k_b \gg k_f$.

3.3.2 Dynamic model fish robot with folding fins

In this subsection, an establishment of the mathematical model of the robot body motion and the folding fins is implemented. The analytical diagram of swimming motion in the 2D platform is illustrated in Figure 3.6.

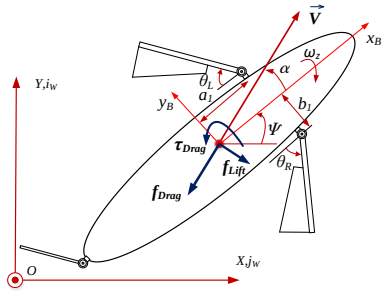

Figure 3.6 Schematic diagram of the robotic fish motion

To account for the motions of the fin panels and the hinge bases, the Lagrange method is employed. Firstly, the kinetic energy of the pectoral fin hinge base is provided by:

$$T_{HK} = \frac{1}{2} m_H v_{CHK}^T v_{CHK} + \frac{1}{2} \omega_{HK}^T \Xi_{HK} \omega_{HK}. \tag{3.11}$$

Secondly, the kinetic energy corresponding to the fin panel component k^{th} of the fin K is described by:

$$T_{Kk} = \frac{1}{2} m_F v_{CKk}^T v_{CKk} + \frac{1}{2} \omega_{Kk}^T \Xi_{Kk} \omega_{Kk}. \tag{3.12}$$

The total of the potential energy of the fin panels can be attained in the following form:

$$P_K = \frac{1}{2} \sum_{k=1}^{2} k_\gamma \gamma_{Kk}^2 + m_{BG} g c_d \left(\cos(\gamma_{K1}) - \cos(\gamma_{K2}) \right). \tag{3.13}$$

Finally, Lagrange function, total virtual work, and Lagrange expression representing the pectoral fin motion are exhibited in followingly corresponding equations:

$$L = T_{HL} + T_{HR} + \sum_{k=1}^{2} \left(T_{Lk} + T_{Rk} - \left(P_{Lk} + P_{Rk} \right) \right), \tag{3.14}$$

$$\delta W = \delta W_L + \delta W_R + \sum_{k=1}^{2} \left(\delta W_{Lk} + \delta W_{Rk} \right), \tag{3.15}$$

$$\frac{d}{dt} \left(\frac{\partial L}{\partial \dot{q}_f} \right) - \frac{\partial L}{\partial q_f} = \frac{\partial \delta W}{\partial \delta q_f}, \tag{3.16}$$

here $\delta W_K = \left(\tau_K + M_K^{shaft} - b_M \dot{\theta}_K\right)\delta\theta_K$; $\delta W_{Kk} = \left(M_{Kk} - b_f \dot{\gamma}_{Kk}\right)\delta\gamma_{Kk}$; b_M and b_f are, respectively, the damping coefficients of mechanical transmission and flexible joints; τ_L and τ_R indicate the torques of left and right motors to produce cyclical motion for the pectoral fins, respectively; $q_f = \left[\theta_L, \gamma_{L1}, \gamma_{L2}, \theta_R, \gamma_{R1}, \gamma_{R2}\right]^T$ denote the generalized coordinates.

3.3.3 Motion control of the folding pectoral fins

An advanced amplitude modulation mechanism-based form will be interchanged to the torque trajectory and expressed by:

$$\begin{cases} \tau_R = \tau(t)\left(1 + k_\Delta\left(\theta_R - \theta_R^{ref}\right) sign\left(\tau(t)\right)\right) \\ \tau_L = -\tau(t)\left(1 + k_\Delta\left(\theta_L - \theta_L^{ref}\right) sign\left(-\tau(t)\right)\right) \end{cases}, \tag{3.17}$$

where θ_R^{ref}, and θ_L^{ref} indicate the reference angles of the right fin and left fin, respectively. For convenience, the reference angles of the fin directions are determining by: $\theta_R^{ref} = 90^\circ, \theta_L^{ref} = -90^\circ$; k_Δ signifies the proportional coefficient and are determined by $k_\Delta = 0.48$.

CHAPTER 4 EXPERIMENTS

4.1 Experimental works concerning the fish robot with the non-uniform pectoral fins

4.1.1 Experimental measurement of robot motion

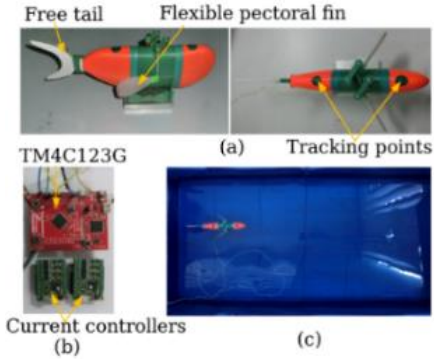

Figure 4.1 The experimental apparatus: The manufactured robot model (a), the primary electronic elements (b), laboratory water tank (c)

In this subsection, the experimental apparatuses for straight swimming mode and turning one are illustrated. Figure 4.1 depicts the robot prototype and concerning equipment.

4.1.2 Estimation of natural frequencies and mode shape functions of non-uniform fins

To estimate the natural frequencies and mode shape functions, the experiments on fins, which are fabricated by the silicone rubber material, are conducted. A comparison among Ansys analysis, Inventor simulation, and the results from the Rayleigh-Ritz method is combined. The objective of this work to converge the result values as well as to reduce the calculated errors.

4.1.3 Estimation of the internal damping of flexible non-uniform fins

The internal damping plays a significant role in the designs of flexible fins. In this consideration, it is assumed that the fin damping is a proportional one. It implies that the matrix of damping can be represented by $C_f = \alpha_1 M_f + \alpha_2 K_f$. Where M_f and K_f denote the mass and stiffness matrixes in the mathematical expression of the flexible fin with its clamped hinge peduncle. α_1 and α_2 are the constants that are determined by the measurement experiments of free vibration in the air. To reduce calculating complexity, assume that the second damping ratio and the first one are equal. The resulting coefficients are included as follows $\alpha_1 = 10.9883$ and $\alpha_2 = 0.0007$.

4.1.4 Measurement of thrust coefficient C_T

To estimate the average propulsive coefficient of a fin, an experiment was carried out with the support of the high-speed camera Casio ZR1000. Its value is calculated from the expression $C_T = 2\left(\int_0^{T_0} F_{thrust}\,dt\right) \Big/ \left(\rho_h A_f \int_0^{T_0} \dot{\chi}_f^2\,dt\right)$, where T_0 is the average measured time. The obtained average outcome and the standard deviation are 0.298 and 0.029, respectively.

4.1.5 Other dynamic coefficients of the robot with non-uniform fins

To provide an additional view for dynamic relationship regarding the motion of the body and the fins deformation, the drag force coefficient C_D, the lift force

coefficient C_L, and the drag moment coefficient C_M are also determined. C_D is estimated by the measurement of the passive straight motion of the robot meanwhile, C_L and C_M are determined through fitting data of the turning swimming mode. Furthermore, by optimizing the fitting data between simulation and experiment, the coefficients of C_d and C_a are discovered by the following approximate description:

$$\begin{cases} C_d = C_{1d} f + C_{2d} T_m + C_{3d} \\ C_a = C_{1a} f + C_{2a} T_m + C_{3a} \end{cases}. \tag{4.1}$$

The result parameters respectively achieved as follows: $C_{1d} = 0.0092$, $C_{2d} = -85.3750$, $C_{3d} = 3.9982$, $C_{1a} = -0.1420$, $C_{2a} = 45.1392$, and $C_{3a} = 0.3555$.

4.2 Experimental setup and the parameters determination of the fish robot with folding fin

4.2.1 Experimental setup of the motion measurement of the robotic fish

The prototype of the fish robot with folding fins is demonstrated in Figure 4.2. It should be noted that the fin panels are equipped with inclination sensors to capture their angular position.

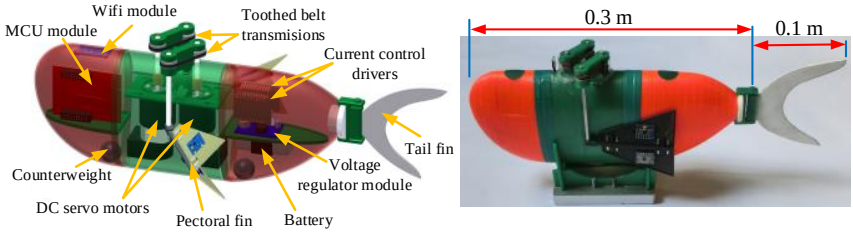

Figure 4.2 The designed fish robot model with a pair of folding fins (a), the fabricated prototype (b)

4.2.2 Estimation of stiffness and damping coefficients of flexible joint

It may be reasonably assumed that the stiffness and the damping coefficients of joints are considered as constants. Thus, the joint's equivalent coefficients of stiffness and damping are directly inferred from experimental measurements of

deformation angle and decay rate of under-damping vibration of a rotating fin panel in the air environment. The result values of four distinct joint prototypes are used in comparison and evaluation of the next Chapter.

4.2.3 Determination of stroke ratio and amplitude ratio of stimulating moment

The relationship among stroke ratio (ε_T), amplitude ratio (ε_P), and forwarding swimming velocity was investigated with prototype T2 at frequency 0.5 Hz. The results show that the robot obtains the highest experimental speed with $\varepsilon_T = 1$ and $\varepsilon_P = 3$. These ratios are applied for testing free-swimming modes then.

4.2.4 Determination of other coefficients

To discover different coefficients consisting of C_L, C_M, C_a, and C_d, identification is conducted by matching responses between simulation and experiment in the turning swimming mode.

CHAPTER 5 RESULTS AND DISCUSSION

5.1 Performance of fish robot with uniform pectoral fin

For demonstrating the feasibility of the proposals, the simulation of swimming motions is shown. In Figure 5.1(a), the traveling direction converges to the reference angle relatively fast. The settling time is about 12 seconds. Furthermore, Figure 5.1(b) describes the performance of the surge velocity, which tracks following the reference speed curve. It should be noted that the speed response's settling time is lower than the heading angle's one, which is only 10 seconds.

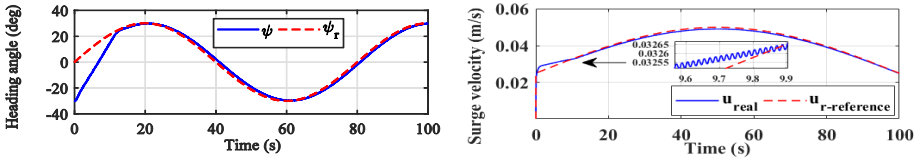

(a) (b)

Figure 5.1 The performances of the direction angle (a) and the surge velocity (b)

Generally, in combination between Lyapunov's stabilization theory and the Hammerstein-Wiener model, the control issue of the robot becomes simpler. The recommended dynamic model of the robot and the designed controller showed the swimming performances relatively well by simulations.

5.2 Performance of fish robot with non-uniform fins

First, to assess the transient response of the robot, the experimental swimming behavior is compared to the simulation one. An indicative example, which is illustrated in Figure 5.2, is conducted at a frequency of $f = 1.5\,\text{Hz}$ and the amplitude of $T_m = 0.008\,\text{Nm}$. The illustrative figures revealed that the recommended model predicts the responses of the surge velocity and the angles of hinges relatively properly. The neutral angles of the flexible fins are stably retained close to the reference angles, which are fixed on $\theta_{dR} = 30^\circ$ and $\theta_{dL} = -30^\circ$, respectively. Moreover, Figure 5.2(d) describes the instantaneous deflection of the fin-tip point of the pectoral fin K, which lags the phase behind the corresponding hinge angle.

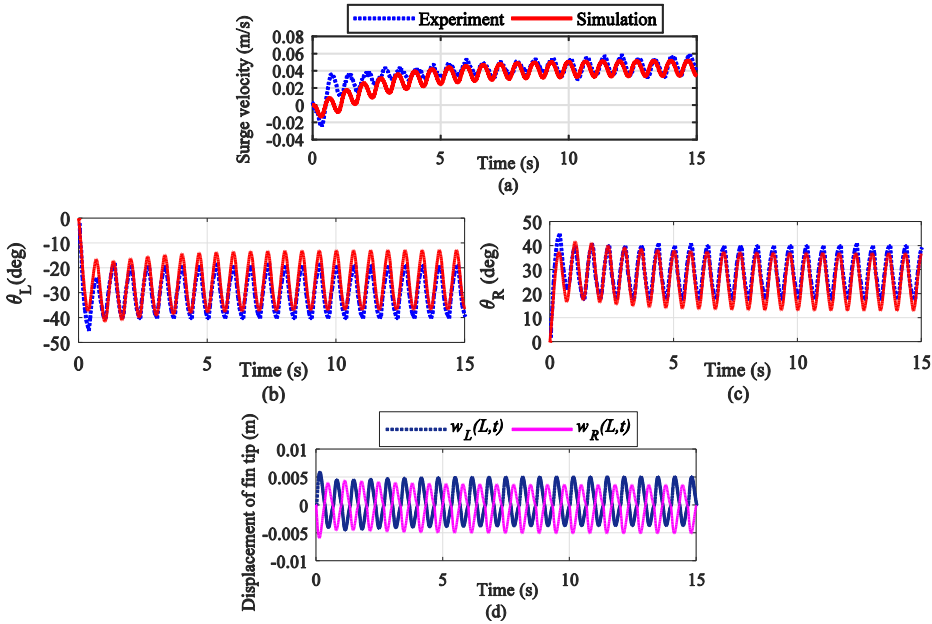

Figure 5.2 The surge velocity performance (a); the rotational angles of the left hinge (b) and the right hinge (c); the fin tip simulation displacement (d)

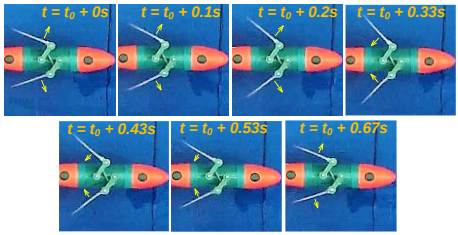

Figure 5.3 Experimental demonstration of movement and deflection of flexible pectoral fins in one cycle

In addition to having an intuitive illustration, Figure 5.3 exhibits the robot's swimming behavior with two pectoral fins in a beating cycle. The trace of the fin tip over time, which is denoted by $w_K(L,t)$, is additionally employed to evaluate the reasonableness in the proposed model. By directly measuring each image frame, the maximum of the experiment deflection of fin tip is smaller 0.008 meters while its magnitude, in simulation, is 0.005 meters. The relative error, which is delineated by the ratio of the absolute deformation error to the length of the compliant fin part, is near 3.7%.

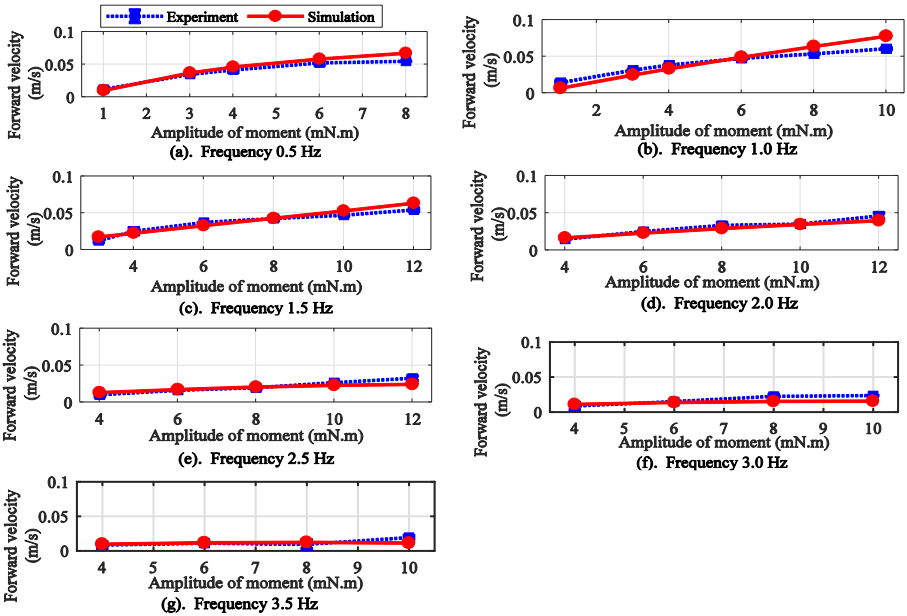

Figure 5.4 The velocity of the robot in the variation of the frequency and amplitude of stimulating moment

Second, to further verify the recommended model, the robot behavior in the steady-state is also examined. The illustration is shown in Figure 5.4. The influences of the frequency and the moment amplitude on the swimming speed are pretty explicit. The higher the moment amplitude employs, the faster the robot movement achieves. At the same condition of moment amplitude, the straight swimming speed decreases while raising the frequency. Moreover, to quantify the discrepancy between the simulation and experiment responses, the mean of absolute straight speed error is observed (see Table 5.1). It should be noted that these values are relatively small. The highest amount of absolute errors takes 0.008 m/s at a frequency of 1.0 Hz. Hence, the discrepancy between the simulation speed and the experiment is quite small.

Table 5.1 Average values of absolute straight velocity errors

$f\,(Hz)$	0.5	1.0	1.5	2.0	2.5	3.0	3.5
$\bar{e}_V^{str}\left(10^{-3} ms^{-1}\right)$	5.3	8.0	4.5	3.1	3.4	4.7	3.2

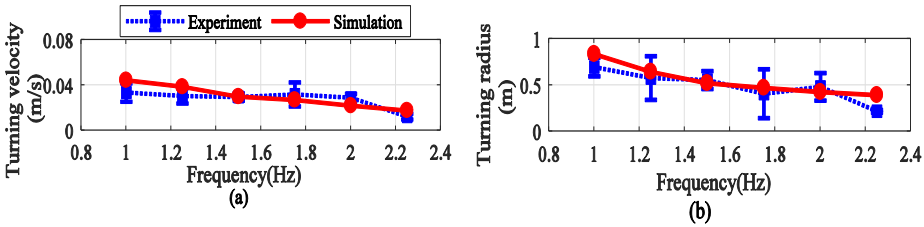

Figure 5.5 Responses of the turning swimming speed (a) and the turning swimming radius (b)

In the turning swimming mode, the responses of swimming speed and turning radius, which is exhibited in Figure 5.5, are also investigated. Generally, the tendency of turning swimming speed and turning radius decreases magnitude while increasing the frequency. Furthermore, the average values of absolute error between simulations and experiments in correspondence with the turning swimming velocity and the turning radius reach 0.006 m/s and 0.089 m. The magnitude of these errors is relatively small while comparing to the corresponding values of turning speed and the turning swimming radius. As a

result, the recommended dynamic model reveals that it can simulate the behavior of robot fish quite fully.

5.3 Performance of fish robot with folding pectoral fins

5.3.1 Influence of the fin joint flexibility on the swimming behavior of the robot

The flexible joint stiffness influences directly on the responses of swimming velocity and turning radius. It is demonstrated through the experimental works on four the different prototypes of flexible joints at the same condition of the testing moment amplitude and frequency from 0.5 to 2.25 Hz. Figure 5.6 and Figure 5.7(a) report the robot speeds corresponding to the forward swimming and turning swimming in both m/s and BL/s (body length per second).

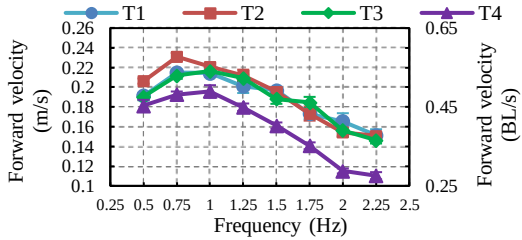

Figure 5.6 The empirical responses of the straight swimming speed in correspondence with the fabricated fin types

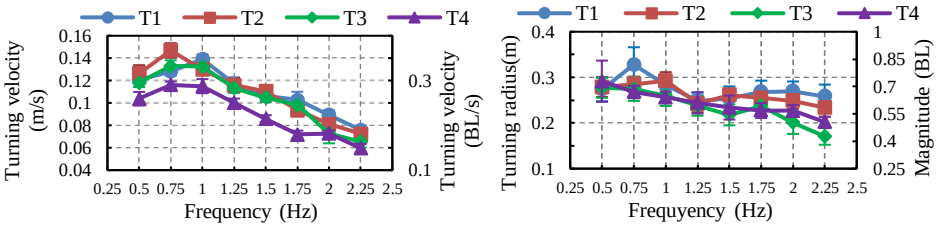

(a) (b)

Figure 5.7 The relationships between the turning swimming speed and the frequency in correspondence with the fin prototypes (a), the experimental turning radius response via the frequency (b)

The captured straight swimming speeds receive the highest values in the narrow range of frequency from 0.75 to 1 Hz. The type T2 can touch the highest speeds of 0.231 m/s (0.58 BL/s) and 0.147 m/s (0.37 BL/s) in correspondence with the

straight swimming mode and the turning one. It is worth mentioning that the peaks of velocity responses locate in the low-frequency region. In another consideration, the relationship of turning radius versus frequency in correspondence with the pectoral fin types is presented in Figure 5.7(b). In general, the radius values decrease as frequency rises. This comparison also reveals that the robot with less flexible joints can achieve higher maneuverability.

5.3.2 Swimming performance of the robot in the transient state

To further evaluate the proposed dynamic model in transient status, the pectoral fin-type T2 is considered due to its remarkable swimming performances. The simulations at the swimming frequency of 0.75 Hz are performed with the same fin type. A comparison between the responses in simulation and experiment is conducted by observing instinctively and calculating normalized Root Mean Squared Error (nRMSE). The coefficients C_a and C_d are adjusted by the trial-error method to fit simulation responses with experimental ones. As a result, their values receive as follows $C_a = 0.15$, and $C_d = 1.62$, respectively.

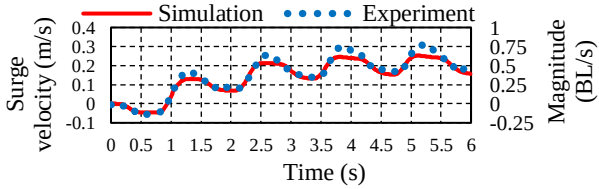

Figure 5.8 The response of the surge swimming speed

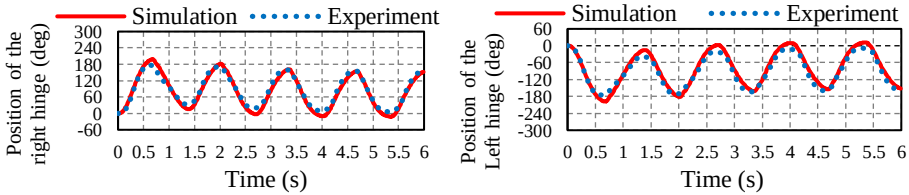

(a) (b)

Figure 5.9 The hinge base position: The right hinge (a), The left hinge (b)

For demonstration, Figure 5.8, Figure 5.9, and Figure 5.10 exhibit the transient performances of the surge speed, the hinge angle, and the fin panels' angles,

respectively. The robot's peak experimental velocity can reach 0.308 m/s (0.78 BL/s) while only using pectoral fins. The results also revealed that the fin hinge motion almost covers the body side area. These results may be a possible explanation for the robot to achieve high speed.

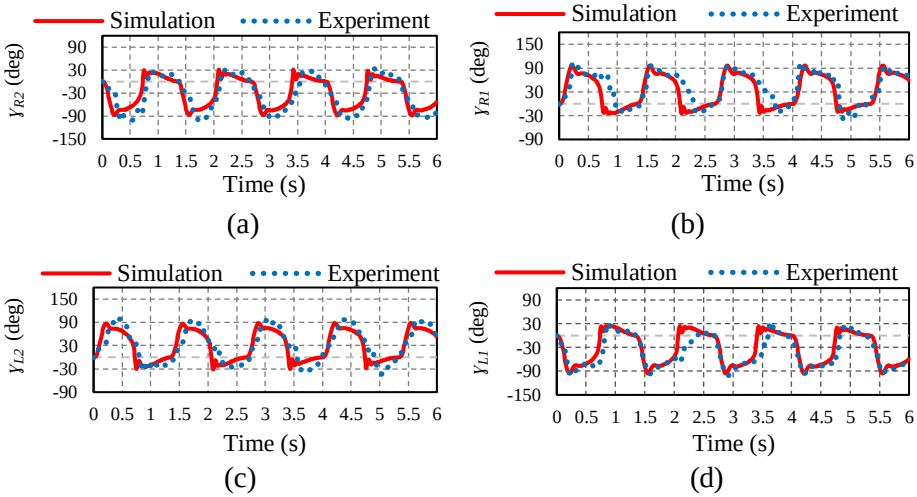

Figure 5.10 The response of angular positions of the fin panels in the comparison between simulations and experiments: under right fin panel (a), upper right fin panel (b), under left fin panel (c), upper left fin panel (d)

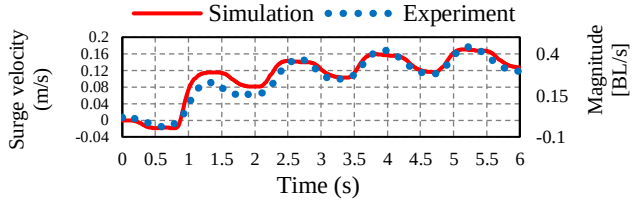

Figure 5.11 The response of the surge swimming speed

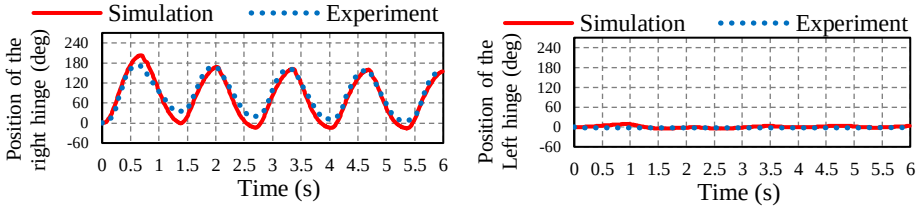

Figure 5.12 The hinge position: the right hinge (a), the left hinge (b)

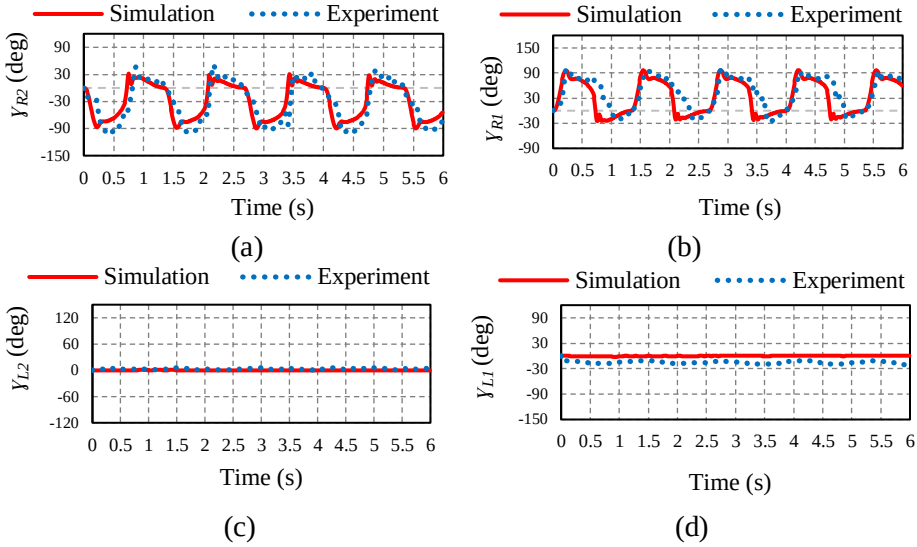

Figure 5.13 The responses comparison of rotational angles of the fin panels between simulations and experiments: under right fin panel (a), upper right fin panel (b), under left fin panel (c), upper left fin panel (d)

The right-turning swimming responses of the robot, in the transient status, are demonstrated in Figure 5.11, Figure 5.12, and Figure 5.13. It is straightforward to perceive that there are high similarities between the experimental results and simulation ones unveiled in both the turning speed and the hinge angles. However, small errors still exist in the angle response of the panels.

5.3.3 Swimming performance of the robot in the steady-state

To additionally evaluate the robot's steady-state performance, the values of nRMSEs, listed in Table 5.2, are examined. In the straight swimming mode, the indexes of nRMSE are relatively small. These declared that the experimental behaviors strongly coincide with the simulation ones. However, the nRMSE index of the left hinge angle is appreciably higher than the others. The reason for this is probably due to the free drift of the left fin position caused by fluid disturbance.

Table 5.2 The nRMSE indexes of the investigated parameters

Mode	Δv_x	$\Delta\theta_R$	$\Delta\theta_L$	$\Delta\gamma_{R1}$	$\Delta\gamma_{R2}$	$\Delta\gamma_{L1}$	$\Delta\gamma_{L2}$
Straight swimming	0.0039	0.0068	0.0076	0.0294	0.0301	0.0221	0.0298
Turning	0.0044	0.0097	0.0939	0.0314	0.0342	0.0419	0.0330

The average surge velocities corresponding to the straight swimming and turning swimming modes are depicted in Figure 5.14 and Figure 5.15(a). In both two performances, it should be noted that the surge speed value rises and obtains the highest magnitude at the frequency of 0.75 Hz, then declines along with the growth of the rowing frequency. The mean relative errors of surge speeds are 8.9% and 15.8%, corresponding to the forward swimming and turning modes.

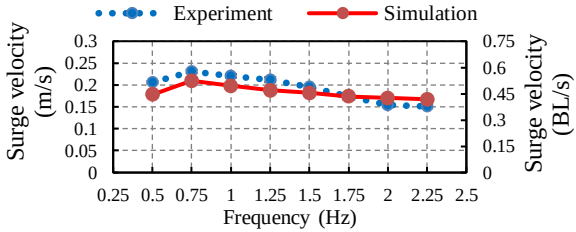

Figure 5.14 Straight swimming speed responses in the comparison between simulation and experiment

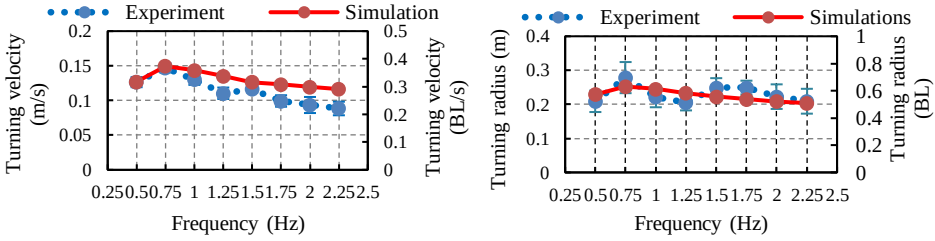

Figure 5.15 The turning swimming speed response in the comparison between simulation and experiment (a), The responses of turning swimming radius in the correspondence between simulation and experiment (b)

Figure 5.15(b) describes the response of the turning swimming radius in relation to the frequency. It is straightforward to see that the change of the mean turning radius over the frequency is quite small. The average relative error is only 9.5%. Generally, the obtained results have led us to the conclusion that the

recommended analytical approach successfully forecasted the locomotion performance of the actual robotic fish.

*5.3.4 Expenditure power, cost of transport (*COT*), propulsive efficiency, and Strouhal number*

For the demonstration, the responses to the power input and COT concerning the frequency are provided in Figure 5.16(a). It unveils that the total of the power input is quite low, smaller than 102 mW, while COT lies in the range of 0.42 - 0.58 (J/kg/m) or 0.17 - 0.23 (J/kg/BL). The value of COT is in a range from 0.10 to 0.27 (J/kg/BL) of a few fish employing median paired fin (MPF) at the similarly swimming speed range (Kendall et al. 2007).

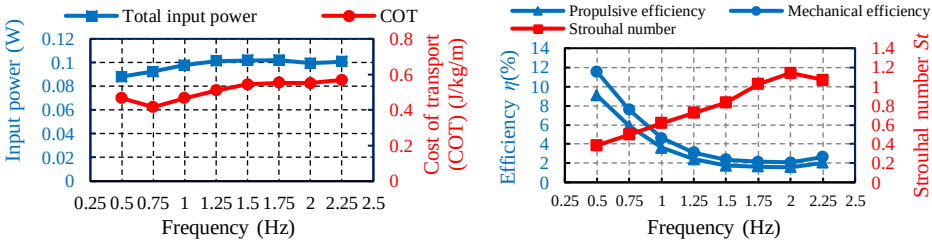

(a) (b)

Figure 5.16 The expenditure power and COT in the forward swimming form (a), The responses, in the straight movement form, of the total thrust efficiency, mechanical efficiency, and Strouhal number (b)

The robot's swimming efficiencies are exhibited in Figure 5.16(b). It should be noted that the highest mechanical efficiency is 11.53%, lower than some earlier reports as 16% of drag based Labriform fish (W. Blake 1980), 31% or 36% corresponding to propulsive efficiency with rigid rays or flexible rays (Shoele and Zhu 2010). Moreover, Figure 5.16(b) depicts the performance of the Strouhal number concerning the frequency. At a frequency 0.75 Hz, the Strouhal number is $St = 0.5$, which locates in the optimal swimming range from 0.15 to 0.8 (Eloy 2012). Finally, to more claim outstanding of recommended fin-type, a swimming behavior comparison between my research and previous researches, which is reported in Table 5.3, is conducted. The speed and maneuverability of my robot are very competitive. Furthermore, the Strouhal number performance also lies

close to the optimal locomotion range of natural fish. However, the swimming efficiency of the robot is not sufficiently high compared to the biology counterpart. Therefore, this is a challenging issue in my next research.

Table 5.3 A response comparison of swimming velocity and turning radius with previous searches

Refs	Maximum average speed		Average turning radius	
(Behbahani and Tan 2017)	0.045 m/s	0.33 BL/s	0.16 - 0.18 m	1.07-1.2 BL
(Behbahani and Tan 2016a)	0.040 m/s	0.2667 BL/s	0.16 - 0.23 m	1.07-1.53 BL
(Behbahani and Tan 2016b)	0.045 m/s	0.3 BL/s	0.23 - 0.24 m	1.53-1.6 BL
(Sitorus et al. 2009)	0.035 m/s	0.09 BL/s	-	-
My research	**0.231 m/s**	**0.58 BL/s**	0.25 - 0.33 m	**0.63-0.83 BL**

CHAPTER 6 CONCLUSIONS

This dissertation dealt with a novel aspect concerning the propulsive mechanism of fish robots with pectoral fins. It also employed many different methods, like the Bernoulli beam theory, the Morison formula, rigid body dynamics, and the Rayleigh-Ritz and the Lagrange methods, to construct mathematical models of motions. Contributions and the next research directions are reported following.

6.1 Contribution

Natural fish is the master of outstandingly swimming skills. Inspired by the morphology of pectoral fin types, maneuverability, swimming speed, and energy usage efficiency of live counterpart, this dissertation presents novel findings to the fish-like robot employing the pectoral fins. Contributions are shown in some aspects as follows:

Firstly, the modeling approach for the fish robot using uniform fin was considered. Where Euler-Bernoulli beam theory, which was combined with the Morison formula, Rayleigh-Ritz method, is key to describe the deflection of pectoral in the fluid. In particular, the control law, which is quite simple, to track the variation of direction and swimming speed was also suggested. The outcomes claimed the reasonability through simulations.

Secondly, inspired by the non-uniform shape of natural fish's pectoral fins, the robot's designs employing pectoral fins as mainly propulsive actuators and their mathematical model were recommended. The analyses of the body motion and fin deformation based on the Rayleigh-Ritz method, Lagrange approach, and Morison formula, were expressed distinctly. The prediction model enabled to represent the real behavior of the robot relatively fully.

Thirdly, the novel type of pectoral fins was proposed, which significantly boosted the ratio between the thrust force and drag force, swimming speed, and maneuverability at a low range of frequencies. The robot's kinematic performance is close to its biological counterpart. The structure of the fin was inspired by the flexible motion and fundamental shape of natural fish.

Finally, as a notable contribution, the analytical model for robotic fish equipped folding fins was recommended. Proposals proved that it could broadly predict locomotion behaviors of the real prototype. This model can be directly used in the designs of motion controllers or to verify the control algorithm.

6.2 Future works

Based successful setup of a mathematical model for the 2D motion of the robot, several extensive works, in the future, will be addressed as follows: Firstly, a dynamic model for the fish robot employing folding fin will be established, where compliant plates replace panel fins. This work will aim to discover challenges in improving swimming efficiency. Secondly, modeling of the robot motion in 3D space will be investigated. However, instead of using a slide-block structure to change the robot's central mass or assistant fins to adjust the pitch attack angle, the pectoral fins will be employed to vary direction to thrust force as well as generate the main propulsive power. Finally, the optimization of swimming speed will be regarded in the constraint of fixed expenditure energy. Furthermore, control issues to mimic the locomotion behavior of natural fish may be considered.

LIST OF PUBLICATIONS

International journals/Book series (ISI-Scopus)

J1. **Van Anh Pham**, Tan Tien Nguyen, Byung Ryong Lee, and Tuong Quan Vo, "Dynamic Analysis of a Robotic Fish Propelled by Flexible Folding Pectoral Fins," *Robotica*, vol. 38, no. 4, pp. 699–718, 2020. (doi: 10.1017/S0263574719000997, **SCIE, IF=1.509, H index=62, SJR=0.4, Q2**)

J2. **Van Anh Pham**, Tan Tien Nguyen, and Tuong Quan Vo, "Dynamically Propulsive Model of a Fish Robot with Flexible Non-Uniform Pectoral Fins," *Journal of Mechatronic Systems and Control*, pp 1-9, 2020. (**ESCI**, **H index=18, SJR=0.25, Q3**)

J3. **Van Anh Pham**, Tan Tien Nguyen, and Tuong Quan Vo, "Modeling and Evaluating Motion Performance of Robotic Fish with a Pair of Non-Uniform Pectoral Fins," *Lecture Notes in Electrical Engineering*, vol. 465, pp. 686-695, 2018. (doi:10.1007/978-3-319-69814-4_66, **H index=28, SJR=0.14, Q3**)

J4. **Van Anh Pham**, Khac Anh Hoang, Tan Tien Nguyen, and Tuong Quan Vo, "A Study on Moving Direction and Surge Velocity Control of a Carangiform Fish Robot Driven by Flexible Pectoral Fins," *Lecture Notes in Electrical Engineering*, vol. 371, pp. 769-778, 2016. (doi:10.1007/978-3-319-27247-4_64, **H index=28, SJR=0.14, Q3**)

National journals

J5. **Van Anh Pham**, Khac Anh Hoang, Tan Tien Nguyen, and Tuong Quan Vo, "An approach of modelling and trajectory tracking control of a robotic fish using soft pectoral fins," *Vietnam Mechanical Engineering Journal*, special issue, pp. 97-103, 2016.

Proceedings of the international conferences

C1. **Van Anh Pham**, Tan Tien Nguyen, and Tuong Quan Vo, "Turning motion direction of fish robot driven by non-uniform flexible pectoral fins," in *2018 2nd International Conference on Recent Advances in Signal Processing, Telecommunications & Computing (SigTelCom)*, Ho Chi Minh, Viet Nam, pp. 29-34, 2018. (doi:10.1109/SIGTELCOM.2018.8325800, **IEEEXplore**)

C2. **Van Anh Pham**, Tan Tien Nguyen, and Tuong Quan Vo, "Hydrodynamic modeling of pectoral fin having varying thickness for biomimetic fish robot," in *2017 7th IEEE International Conference on System Engineering and Technology (ICSET)*, Shah Alam, Malaysia, pp. 89-94, 2017 (doi:10.1109/ICSEngT.2017.8123426, **IEEEXplore**)

C3. **Van Anh Pham**, Tan Tien Nguyen, and Tuong Quan Vo, "The Influence of Non-Uniform Flexible Pectoral Fin Thickness to Velocity Performances of Robotic Fish," in *2017 the 4th Vietnam Internation Conference and Exhibition On Control and Automation (VCCA)*, Ho Chi Minh, Vietnam, 2017.

C4. **Van Anh Pham**, Tan Tien Nguyen, and Tuong Quan Vo, "A Study on a Type of Bionic Pectoral Fin of Carangiform Robotic Fish in Flapping Mode," in *the South*

East Asean Technical University Consortium Symposium, Ho Chi Minh, Vietnam, 2017.
C5. **Van Anh Pham**, Khac Anh Hoang, Tan Tien Nguyen, and Tuong Quan Vo, "A Modelling Approach for Soft Pectoral Fins of a Carangiform Fish Robot," in the *7th TSME International Conference on Mechanical Engineering*, Chiang Mai, Thailand, 2016.

Proceedings of the national conferences
C6. **Van Anh Pham**, Tan Tien Nguyen, and Tuong Quan Vo, "The Flexible Pectoral Fin for Fish Robot: A Modeling Approach and Propulsive Efficiency Comparision Between Several Fin Types," in *8th National Conference on Mechatronics (VCM)*, Vietnam, 2016.
C7. **Van Anh Pham**, Khac Anh Hoang, Tan Tien Nguyen, and Tuong Quan Vo, "A Study on Flexible Pectoral Fins Modelling of a Carangiform Fish Robot " in *National Conference on Machines and Mechanisms (NCOMM)*, Ho Chi Minh, Vietnam, pp. 163-172, 2015.
C8. **Van Anh Pham**, Khac Anh Hoang, Tan Tien Nguyen, and Tuong Quan Vo, "A Swimming Hydrodynamic Model of Carangiform Robotic Fish Driven by Flexible Pectoral Fins," in *National Conference on Machines and Mechanisms (NCOMM)*, Ho Chi Minh, Vietnam, pp. 93-102, 2015.

Other related publications
J6. Khac Anh Hoang, **Van Anh Pham**, Tan Tien Nguyen, and Tuong Quan Vo, "A Study on Controllers Design of a 3-Joint Carangiform Fish Robot in 3D Environment," *Lecture Notes in Electrical Engineering*, vol. 371, pp. 791-802, 2016. (doi:10.1007/978-3-319-27247-4_66, **H index=28, SJR=0.14, Q3**)
J7. Khac Anh Hoang, **Van Anh Pham**, Tan Tien Nguyen, and Tuong Quan Vo, "A Study on Development of the Dynamics System of a 3-Joint Carangiform Fish Robot in Horizontal Plane," *Vietnam Mechanical Engineering Journal*, special issue, pp110-115, 2016.
J8. Khac Anh Hoang, **Van Anh Pham**, Tan Tien Nguyen, and Tuong Quan Vo, "The New Dynamic Analysis Approach and Trajectory Following Control of A Carangiform Fish Robot," *Journal of Technical Education Science*, issue 33, pp. 66-77, 2015.
C9. Khac Anh Hoang, **Van Anh Pham**, Tan Tien Nguyen, and Tuong Quan Vo, " The new dynamic for tail of 3-joint Carangiform robotic fish," in *National Conference on Machines and Mechanisms (NCOMM)*, Ho Chi Minh, Vietnam, pp. 103-112, 2015.

Related research projects
P1. Modeling and control pectoral fins for fish robot Carangiform, (TNCS-CK-2015-13). (Main author)
P2. Research new methods in dynamic analysis and motion control for fish robot Carangiform, (TNCS-2015-CK32). (Co-author)